Magnetic excitations in vanadium spinels

N. B. Perkins[1,2] and O. Sikora[3]
[1]*Institute fur Theoretische Physik, TU Braunschweig, Mendelssohnstrasse 3, 38106 Braunschweig, Germany*
[2]*Department of Physics, University of Wisconsin, Madison, Wisconsin 53706, USA*
[3]*MPIPKS, Nöthnitzer Strasse 38, 01187 Dresden, Germany*
(Received 21 June 2007; revised manuscript received 25 September 2007; published 28 December 2007)

We study magnetic excitations in vanadium spinel oxides AV_2O_4 (A=Zn,Mg,Cd) using two models: the first one is a superexchange model for vanadium $S=1$ spins and the second one includes, in addition, spin-orbit coupling and crystal anisotropy. We show that the experimentally observed magnetic ordering can be obtained in both models; however, the orbital ordering is different with and without spin-orbit coupling and crystal anisotropy. We demonstrate that this difference strongly affects the spin-wave excitation spectrum above the magnetically ordered state, and argue that the neutron measurement of such dispersion is a way to distinguish between the two possible orbital orderings in AV_2O_4.

DOI: 10.1103/PhysRevB.76.214434 PACS number(s): 75.10.Jm, 75.30.Ds

I. INTRODUCTION

Due to geometrical frustration, transition metal spinel oxides with a general formula AB_2O_4 display a variety of unusual low-temperature properties. The spin dynamics of these systems is usually described by a Heisenberg antiferromagnet on the pyrochlore lattice. This model is rather peculiar and its classical ground state is highly degenerate. Exact degeneracy can be lifted by various mechanisms, but the system still possesses many competing spin configurations with almost equal energies. As a result, when the temperature goes down, the system can evolve in a variety of ways: it can remain spin liquid down to the lowest temperatures due to quantum fluctuations, or choose a particular configuration either via the strongest order from disorder mechanism or through a structural phase transition which lowers the local symmetry of the lattice.

A peculiarity of transition metal spinels is that their magnetic ions often possess also an orbital degree of freedom. This extra degree of freedom modulates the spin exchange and can at least partially lift the geometrical degeneracy of the underlying lattice. However, the orbital degrees of freedom in geometrically frustrated lattices are by themselves frustrated, i.e., many different orbital configurations have the same energy. In this situation, the ordering in the orbital sector is coupled to the ordering in the spin sector, and the selection of a true ground state configuration becomes a nontrivial phenomena.

Of particular interest is the orbital ordering in the t_{2g} systems on the pyrochlore lattice. In this work, we study vanadium spinels of the type AV_2O_4, where A is a divalent ion such as Cd^{2+}, Zn^{2+}, or Mg^{2+}. In these compounds, magnetically active V^{3+} ions form a pyrochlore lattice and have two $3d$ electrons in t_{2g} orbitals. Due to strong Hund's interaction, these two electrons form a state with $S=1$. All AV_2O_4 compounds show qualitatively similar structural and magnetic behavior, independently of what the divalent A ion is, and undergo two phase transitions—a structural one and an antiferromagnetic one. We will be mainly discussing the physics of ZnV_2O_4. The structural transition occurs at a temperature $T_S \sim 50$ K.[1] Below T_S, the lattice shows a tetragonal distortion—the vanadium octahedra VO_6 are uniformly flattened along the c axis, and the symmetry is lowered from the cubic one to $I4_1/amd$, which is the highest-symmetry tetragonal space group for the spinel structure. The antiferromagnetic (AFM) transition occurs at a slightly lower temperature T_N of about 40 K.[2,3] This temperature is significantly lower than the Curie-Weiss temperature $T_{CW} \sim 1000$ K, extracted from high temperature susceptibility,[4] which underlines the importance of geometrical frustration.

The magnetic structure of AV_2O_4 spinels at $T<T_N$ was first proposed by Nizioł[2] and recently confirmed by Reehius *et al.* in Ref. 3. Along the diagonal $[110]/[\bar{1}10]$ direction in the xy plane, the ordering is antiferromagnetic $+-+-\cdots$, while along the two other diagonal directions $[011]/[0\bar{1}1]$ in the yz plane and $[101]/[\bar{1}01]$ in the xz plane, the spin ordering is in the form $++--++--\cdots$ (see Fig. 1).

At high temperatures $T>T_S>T_N$, inelastic neutron scattering data by Lee *et al.*[5] on the powder sample of ZnV_2O_4 still show strong low energy magnetic excitations which form a broad peak centered at $Q=1.35$ Å^{-1}. This broad peak is present also at $T_N<T<T_S$; however, it becomes asymmetric and shifts toward a smaller value of Q. The asymmetry of the peak further increases in the magnetically ordered phase ($T<T_N$).[5] The value of Q and its temperature evolution cannot be explained within a purely spin model, whose funda-

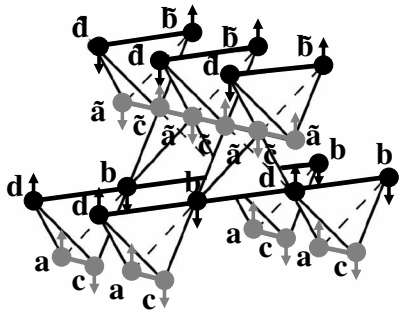

FIG. 1. Magnetic ordering consisting of one-dimensional antiferromagnetic chains in the xy plane. Black and gray colors correspond to the orbital configuration in the ROO state.

mental degrees of freedom are antiferromagnetic hexagonal spin loops with $Q=1.5$ Å^{-1}, which is larger than the experimental Q. The spin dynamics, however, can be understood if one assumes that spin degrees of freedom are affected by the orbital degrees of freedom. In particular, the spatial asymmetry of the peak in the intermediate phase can be understood as the consequence of the fact that at $T<T_S$, vanadium octahedra are flattened and xy orbital at each site is occupied. This leads to a strong antiferromagnetic exchange between vanadium spins along the xy direction, and, as a result, spin interactions become effectively one dimensional. Strong one-dimensional spin fluctuations give rise, via spin-orbit coupling, to fluctuations of the occupations of xz or yz orbitals, causing the anisotropy of the neutron peak.

There were several theoretical attempts to understand the nature of the ground state of ZnV_2O_4. However, although it is widely accepted that orbital degrees of freedom play an important role, no consensus is reached yet about the type of the orbital ordering (OO) in the ground state. The first attempt to explain the physics of ZnV_2O_4 focused on the spin-lattice coupling mechanism;[6] however, it did not explain why the structural and spin order occur at different temperatures. Tsunetsugu and Motome[7] later addressed this issue and related the presence of two separate phase transitions at T_N and T_S to the interplay between geometrical frustration and $dd\sigma$ superexchange (SE) interaction between V ions. The ground state orbital ordering suggested in Ref. 7 consists of stacked ab planes with alternating orbital occupations (xy,xz) and (xy,yz). Hereafter, we label this orbital patterns as ROO. They also showed that this ordering of orbitals can partially remove magnetic frustration and explain experimentally observed ordered magnetic structure.

On the other hand, Tchernyshyov[8] pointed out that the ground state obtained in Ref. 7 is at odds with x-ray and neutron diffraction data because it does not possess the required $I4_1/amd$ space symmetry. He argued that the spin-orbit coupling should be included into consideration. He considered a purely ionic model in which spin-orbit (SO) coupling plays the major role and determines the orbital order in the tetragonal phase. He suggested the following OO: one electron on each site occupies xy orbital, while the second electron is spreaded between xz and yz orbitals in such a way as to minimize the spin-orbit energy at each site. Hereafter, we label this orbital pattern as COO.

Recently, Maitra and Valenti [9] found in the *ab initio* density functional theory calculations that a correct space symmetry can be actually obtained within the reasoning of Ref. 7, if one includes into consideration an additional trigonal distortion. Still, the true ground state turns out to be the same as in Ref. 8.

The ideas of Refs. 7 and 8 were combined in the unique framework by Di Matteo *et al.* in Ref. 10. They proposed to construct a classical ground state phase diagram by considering SE interaction and SO coupling on equal footing. They demonstrated that the SO coupling is a relevant perturbation and favors the states with unquenched orbital momentum for any value of the coupling strength. They obtained a variety of phases and found that for reasonable values of SE and SO couplings, the ground state agrees with the experimentally observed one.

In this paper, we extend the analysis of Ref. 10 and study the low energy excitations in vanadium spinels. We find that the magnetic excitation spectrum strongly depends on the type of the OO, and that it is qualitatively different for the ground states with patterns that consist of real orbitals and those with the complex linear combination of orbitals, i.e., complex orbitals. The former ground state is characterized by a quenched orbital angular momentum $(L=0)$, while the latter by a unquenched $(L\neq 0)$ orbital angular momentum.[11] The difference in the magnetic excitation spectrum arises due to the fact that the magnetic moment of the vanadium ion is formed by both spin and orbital momentum, and fluctuations of $\mathbf{L}$ contribute to the spectrum of magnetic excitations. We argue that the measurement of magnetic excitations in neutron scattering experiments can shed light on the nature of the OO in the ground state.

This paper is organized as follows. In Sec. II, we introduce the model appropriate for the description of the physical properties of ZnV_2O_4. In Sec. III, we discuss the ground state and the magnetic excitations of the system when the orbital angular momentum is quenched. We derive linear spin-wave theory of $S=1$ moments interacting on the V^{3+} pyrochlore lattice. In Sec. IV, we discuss ground state and magnetic excitations of the system when the orbital angular momentum is unquenched. We show that magnetic excitations for unquenched disorder can be described in the framework of the magnetic excitonic model. Section V presents the conclusions. Some mathematical details are given in Appendices A and B.

II. MODEL

The minimal model describing the low energy physics of vanadium spinel is given by

$$H = H_{\mathrm{SE}} + H_a + H_{\mathrm{SO}}. \tag{1}$$

The first term describes nearest neighbors (nn) superexchange interactions between vanadium $S=1$ spins, arising from the virtual excitations $d_i^2 d_j^2 \rightarrow d_i^1 d_j^3$. These interactions can be written as

$$H_{\mathrm{SE}}^{nn} = -\sum_{\langle ij\rangle} [J_0 \mathbf{S}_i \cdot \mathbf{S}_j + J_1] O_{ij} - \sum_{\langle ij\rangle} J_2 [1 - \mathbf{S}_i \cdot \mathbf{S}_j] \bar{O}_{ij}, \tag{2}$$

where i and j are the nearest neighbors, $J_0=\eta J/[1-3\eta]$, $J_1=J[1-\eta]/[1-3\eta]$, $J_2=J[1+\eta]/[1+2\eta]$ are coupling constants, and $J=t^2/U_1$ is the overall energy scale ($t=3/4t_{dd\sigma}$ and U_1 is the intraorbital Coulomb repulsion), with $\eta=J_H/U_1$ the normalized Hund's exchange. We consider only the largest the hopping term, associated with σ bonding.[13] Such hopping is diagonal and nonzero only if the orbitals and the plane in which hopping occurs are of the same $\alpha\beta$ type $(\alpha\beta=xz,yz,xy)$. In this case, orbital contributions O_{ij} and $\bar{O}_{ij}$ are expressed in terms of projectors $P_{i,\alpha\beta}$ onto the occupied orbital state $\alpha\beta$ at sites i and j: $O_{ij}=P_{i,\alpha\beta}(1-P_{j,\alpha\beta})+P_{j,\alpha\beta}(1-P_{i,\alpha\beta})$ and $\bar{O}_{ij}=P_{i,\alpha\beta}P_{j,\alpha\beta}$.

To describe the anisotropy and spin-orbit coupling term, we use the fact that, when the crystal field splitting between t_{2g} and e_g orbitals is large, the t_{2g} electrons can be repre-

sented by an effective orbital angular momentum $L'=1$.[12] The anisotropy term (the second term of the Hamiltonian [Eq. (1)]), is then given by

$$H_a = c\sum_i L'^2_{zi}. \tag{3}$$

where c is a constant. This term describes the tetragonal distortion in the t_{2g} manifold. We notice here that for simplicity, we neglect the trigonal distortion, which is small compared to the tetragonal one.

The spin-orbit coupling term [the third term in Eq. (1)] is given by

$$H_{\mathrm{SO}} = -\lambda\sum_i \mathbf{L}'_i \cdot \mathbf{S}_i, \tag{4}$$

where λ is the SO coupling constant. Note that the true angular momentum $\mathbf{L}$ is related to an effective one as $\mathbf{L}\simeq -\mathbf{L}'$.

The parameters of the model can be estimated from the experiments. The spectroscopy data[14] yield Hund's exchange $J_H\simeq 0.68$ eV and Coulomb intraorbital repulsion $U_1\simeq 6$ eV. The estimate of hopping matrix element from x-ray photoemission spectroscopy is $t\simeq -0.35$ eV,[13] so the energy scale is $J=t^2/U_1\simeq 20.4$ meV. Since the SO coupling constant is $\lambda\simeq 13$ meV (Ref. 15), we can see that the superexchange and the spin-orbit couplings are comparable and, therefore, should be treated on equal footing.

III. REAL ORBITAL ORDER

A. Ground state

First, we discuss the ground state of the superexchange Hamiltonian alone [Eq. (2)]. Without the anisotropy and spin-orbit terms, the ground state orbital patterns consist of only real orbitals: at each site two out of three t_{2g} orbitals xy, xz, and yz are occupied. This type of orbital patterns is called real orbital order, as opposed to complex orbital order, when the orbital state is formed by a complex superposition of t_{2g} orbitals in such a way that the gain of spin orbit interaction energy is maximized.

Depending on which orbitals are occupied, one obtains two types of interacting bonds and also noninteracting bonds. Consider, for example, a bond in the $\alpha\beta$ plane. If there is an electron occupying $\alpha\beta$ orbital only on one site of such bond, then the bond, which we label as b_1, is weakly ferromagnetic and is described by $H_{b_1}=-J_0\mathbf{S}_i\cdot\mathbf{S}_j-J_1$. If both i and j sites of ij bond are occupied by $\alpha\beta$ electrons, then the bond, which we label as b_2, is strongly AFM. The exchange coupling is then given by $H_{b_2}=-J_2(1-\mathbf{S}_i\cdot\mathbf{S}_j)$. When neither i nor j site have $\alpha\beta$-orbital occupied, the bond is noninteracting.

One can easily demonstrate[10] that for positive J_0 and J_2, the lowest energy configuration corresponds to the state with four ferromagnetic b_1 bonds per tetrahedron. There still exist two topologically different tetrahedral configurations with four b_1 bonds, characterized by different OO patterns. One of them, the ROO state with OO patterns proposed by Tsunetsugu and Motome[7] is compatible with experimentally observed magnetic structure—it yields AFM chains running in the [110] and $[1\bar{1}0]$ directions (see Fig. 1). The classical energy per site in the ROO state is $E_{\mathrm{ROO}}=-2J_1-2J_2$. However, this state is actually not the true ground state of the superexchange Hamiltonian [Eq. (2)]. The other state with four b_1 bonds (the ROO-I state in our notations), in which spins of each tetrahedron form a fully collinear up-up-up-down ($uuud$) state, has the ground state energy $E_{\mathrm{ROO\text{-}I}}=-J_0-2J_1-2J_2$, which is lower than that of the ROO state. This is the lowest classical energy that one can obtain within the manifold with quenched angular momentum at each site.[10] However, the magnetic ordering associated with the ROO-I state is incompatible with the experimentally observed one: in ROO-I, two neighboring spins in the xy plane are ferromagnetically aligned, whereas the experimentally detected coupling in the xy plane is antiferromagnetic. This discrepancy between the ROO-I ground state of the superexchange Hamiltonian [Eq. (2)] and the experimental findings demonstrates the necessity of taking into account additional interactions We study the the anisotropy term and the spin-orbit coupling in the Sec. IV.

One can also consider the model with both the SE and the Jahn-Teller (JT) couplings[17] with a hope that the cooperative JT effect, which plays an important role in the structural transition, can also stabilize the ROO type of orbital order. This model has been studied in Ref. 17 by both the mean-field analysis and Monte Carlo simulations. Here, we assume that the ROO phase can be realized and in Sec. III B, we derive magnetic excitations spectrum for the corresponding effective spin model.

B. Spin waves

The starting point for the calculation of the magnon excitation spectrum is the classical Néel ground state with antiferromagnetic spin chains in the xy planes (Fig. 1). This ground state has the magnetic unit cell with eight vanadium spins, which we denote as a, b, c, d, $\tilde{a}$, $\tilde{b}$, $\tilde{c}$, and $\tilde{d}$ (Fig. 1). After averaging the orbital operators, we can rewrite the Hamiltonian [Eq. (2)] as

$$H_{nn} = J_{xy}\sum_{\langle ij\rangle\parallel xy} \mathbf{S}_i\cdot\mathbf{S}_j + J'\sum_{\langle ij\rangle\parallel xz,yz} \mathbf{S}_i\cdot\mathbf{S}_j, \tag{5}$$

where the first term describes the superexchange along the xy chain with $J_{xy}=J_2$, while the second term corresponds to the frustrated ferromagnetic interchain coupling, $J'=J_0$.

To describe the excitation spectrum of such eight-sublattice antiferromagnet, we introduce eight boson operators: a, b, c, d, $\tilde{a}$, $\tilde{b}$, $\tilde{c}$, and $\tilde{d}$. We employ Holstein-Primakoff transformation, e.g., for up spins $\mathbf{S}_a$ and down spins $\mathbf{S}_b$, we have

$$S^z_a = S - a^\dagger a, \quad S^z_b = -S + b^\dagger b,$$

$$S^+_a = \sqrt{2S - a^\dagger a}\,a, \quad S^+_b = b^\dagger\sqrt{2S - b^\dagger b},$$

$$S^-_a = a^\dagger\sqrt{2S - a^\dagger a}, \quad S^-_b = \sqrt{2S - b^\dagger b}\,b. \tag{6}$$

In the linear spin wave approximation, we substitute $\sqrt{2S-p^\dagger p}=\sqrt{2S}$ in the expressions above. Performing Fourier

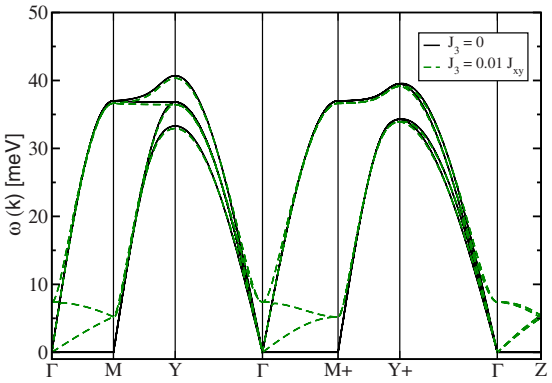

FIG. 2. (Color online) The spin-wave dispersions obtained along the main directions of the 3D BZ. Solid line corresponds to the magnon spectrum when $J_3=0$ and dashed line to the magnon spectrum with the correction due to the third nearest neighbor interaction with $J_3=0.01J_{xy}$. We have used the following labels for high-symmetry points: $\Gamma=(0,0,0)$, $M=(\pi/4,\pi/4,0)$, $Y=(0,\pi/2,0)$, $M+=(\pi/4,\pi/4,\pi/4)$, $Y+=(0,\pi/2,\pi/4)$, and $Z=(0,0,\pi/4)$.

transformation $p_k=\frac{1}{\sqrt{N}}\Sigma_i e^{-i\vec{k}\vec{r}_i}p_i$, where N is the number of lattice sites belonging to one sublattice, we obtain the mean field Hamiltonian for magnons,[16]

$$H=[\mathbf{a}^{\dagger}(\mathbf{k}),-\mathbf{a}(-\mathbf{k})]\begin{pmatrix}\mathbf{A}(\mathbf{k}) & \mathbf{B}(\mathbf{k})\\ -\mathbf{B}(-\mathbf{k}) & -\mathbf{A}(-\mathbf{k})\end{pmatrix}\begin{pmatrix}\mathbf{a}(\mathbf{k})\\ \mathbf{a}^{\dagger}(-\mathbf{k})\end{pmatrix}, \tag{7}$$

where we introduced $\mathbf{a}(\mathbf{k})=(a_{\mathbf{k}},b_{\mathbf{k}},c_{\mathbf{k}},d_{\mathbf{k}},\tilde{a}_{\mathbf{k}},\tilde{b}_{\mathbf{k}},\tilde{c}_{\mathbf{k}},\tilde{d}_{\mathbf{k}})$. The matrices $\mathbf{A}(\mathbf{k})$ and $\mathbf{B}(\mathbf{k})$ are 8×8 matrices whose elements depend on the geometry of the lattice and the type of the magnetic ordering; tilde denotes the complex conjugation. The explicit expression for matrix elements are presented in Appendix A. The quadratic form is diagonalized using the generalized Bogoliubov transformation. In the diagonal form, the Hamiltonian takes the form

$$H_{\mathbf{k},-\mathbf{k}}=H^0_{\mathbf{k},-\mathbf{k}}+\sum_n \lambda_{n\mathbf{k}}b^{\dagger}_{n\mathbf{k}}b_{n\mathbf{k}}+\sum_n \lambda_{n-\mathbf{k}}b^{\dagger}_{n-\mathbf{k}}b_{n-\mathbf{k}}, \tag{8}$$

where the index n runs from 1 to 8, $\lambda_{n\mathbf{k}}=\lambda_{n-\mathbf{k}}$ are the magnon energies, and $b_{n\mathbf{k}}$ are the linear combinations of boson operators belonging to $\mathbf{a}(\mathbf{k})$ and $\mathbf{a}(-\mathbf{k})$.

We obtained the spin-wave excitation spectrum by solving Eq. (8) numerically. The result is presented in Fig. 2 along the high-symmetry directions of three-dimensional (3D) Brillouin zone. We used $J_{xy}=18.5$ meV and the ferromagnetic constant $J'=-0.1J_{xy}$. There are four different branches of the spin-wave spectrum, each of them is doubly degenerate. Furthermore, two of the branches have zero energy over a finite range of momenta [see Fig. 2 (solid lines)]. This so-called zero modes emerge because the number of ferro- and antiferrobonds connecting two neighboring antiferromagnetic chains is the same (see Fig. 1), and the spins forming the xy chains can collectively rotate with no change in energy.

The existence of the zero modes is inconsistent with the observation of the magnetic ordering transition at ~40 K.

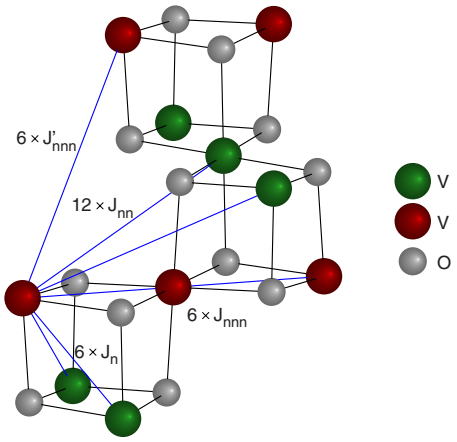

FIG. 3. (Color online) J_n, J_{nn}, and J_{nnn} are first-, second-, and third-neighbor exchange couplings. Second-neighbor interactions J_{nn} are frustrated. The third-neighbor exchange coupling through the empty space we assume equal to zero, $J'_{nnn}=0$; the other coupling are equal to $J_{nnn}=J_3$, only if they connect sites along the direction corresponding to the symmetry of orbital occupation. Red and green colors denoting vanadium ions correspond to orbital configurations in ROO state.

The ordering requires that the zero mode be lifted. The issue is what interactions are responsible for the lifting of spin degeneracy.

A natural first step would be to consider longer range interactions[17] as these interactions generally remove the degeneracy (it happens, e.g., in a kagome antiferromagnet). We show below that it is indeed the case, however, the energy of the relevant degeneracy-breaking mode is very small and cannot explain the magnetic ordering temperature of ~40 K.

In Fig. 3, we show the interactions which include up to third neighbors. There are six nearest neighbor interactions J_n ($J_n=J_{xy}$ along the xy chain and $J_n=J'$ along the xz and yz bonds), 12 second neighbor interactions J_{nn}, and 12 third neighbor interactions J_{nnn}. Quite often already inclusion of the second neighbor exchange lifts the degeneracy. However, here the second-neighbor interactions J_{nn} are frustrated and cannot remove the degeneracy, and therefore, zero modes in the spin-wave spectrum.[17] Thus, one has to include third neighbor exchanges. There are two inequivalent sets of third neighbors, one obtained by two nearest neighbor steps J_{nnn} and the other through the empty space J'_{nnn} (see Fig. 3).

When only $dd\sigma$ hopping is considered, the exchange coupling through the empty space is zero, $J'_{nnn}=0$, and only J_{nnn} interactions contribute. These interactions are antiferromagnetic $J_{nnn}=J_3>0$ and nonzero only if they connect sites along the direction corresponding to the symmetry of the orbital occupation (i.e., for orbital occupation $\alpha\beta$, the interaction is nonzero only along the $\alpha\beta$ direction).

The third neighbor interaction is frustrated along the xy chains, but it is small compared to nearest neighbor exchange along the chain, $J_3\ll J_{xy}$, and cannot destroy antiferromagnetic ordering along the chain. Along the xz and yz directions J_3 are not frustrated and connect parallel antiferromagnetic chains located in second neighboring xy planes. The energy scale for J_3 is then $\frac{t^4_{dd\sigma}}{U_1^3}$. This is a very small

energy, only about 1% of the frustrated ferromagnetic interchain coupling $J' \sim \frac{t_{dd\sigma}^2}{U_1}$. This small interaction cannot explain the magnetic ordering temperature of ~40 K.[18] Here, we consider this interaction only qualitatively and assume the value of coupling constant $J_3=0.01J_{xy}$. One can see in Fig. 2 (dashed lines) that the zero energy modes indeed become dispersive for $J_3>0$.

We would like to note that experimentally it has been proven that all magnetic moments are aligned along the z direction. This experimental fact cannot be explained in the framework of the SE model because it is isotropic in a spin space. In reality, vanadium spinels likely possess a single ion spin anisotropy which aligns spin along the z direction. The anisotropy does affect the magnetic excitation spectrum which in its presence acquires a gap. In this case, the zero mode will be lifted and the spin frustration will be removed. However, since the strength of magnetic anisotropy is not known experimentally at the moment, we cannot estimate the magnitude of the anisotropy-induced gap and check whether or not this interaction alone can stabilize the ground state magnetic structure. We believe that the role of the anisotropy deserves further experimental and theoretical investigation.

IV. COMPLEX ORBITAL ORDER

A. Ground state

We now consider the ground state of the system in the presence of the SO coupling and the anisotropy term [Eqs. (3) and (4)]. For any finite λ, the SO coupling prefers the orbital state with the unquenched effective orbital angular momentum $L'=1$. In such orbital state, one electron at each site occupies the xy orbital due to the tetragonal distortion, while the second electron occupies the complex linear combination of the xz and yz orbitals. The effective $\mathbf{L}'$ should then be parallel to the spin magnetic moment in order to minimize the spin-orbit energy, i.e., a spin-up site will have $L'_z=1$, while a spin-down site will have $L'_z=-1$. As we discussed earlier, this type of orbital ordering is a COO state suggested first by Tchernyshyov in Ref. 8. Its energy $E_{COO}=-1/2[5J_2+2J_1]-\lambda$ is lower than the energy of the ROO state for a wide range of parameters (see the phase diagram in Ref. 10).

The COO state is characterized by two strong AFM bonds per tetrahedra, and its magnetic structure consists of AFM chains in the xy planes with the same interaction along the chain as in the ROO state. The strengths of the interchain coupling J' are also practically the same for the ROO and the COO states,[10] although $J'=1/4[J_2-2J_0]$ is antiferromagnetic in the COO state, while it is ferromagnetic in the ROO state. In this work, we assume $|J'|/J_{xy}=0.1$ in both orbital states. In the COO state, the preferred spin direction is fixed by anisotropy term [Eq. (3)] via the SO coupling to be along the z axis, and therefore, spins in the xy chains cannot rotate freely even for only nearest-neighbor exchange along the chains. The long range order $+\ +\ -\ -\ \cdots$ along diagonal directions in the xz and yz planes cannot be determined by local interactions, but for simplicity, we do not include the next neighbor hopping terms in this part of our calculations.

B. Magnetic excitons

We now consider magnetic excitations in the COO state. We follow the magnetic exciton model approach of Refs. 19 and 20, which is the extension of the linear spin wave theory for systems with unquenched orbital angular moment.

We consider states with the effective total angular momentum $\mathbf{J}=\mathbf{L}'+\mathbf{S}$. Often, energy levels with different J are well separated in energy and both J and its z projection J_z are good quantum numbers. However, in many transition metal oxides, the strength of the spin-orbit coupling and the superexchange interaction between localized d electrons are comparable, and the atomic energy levels with different values of J can cross each other; in such case, only J_z acts as a good quantum number. We show below that magnetic excitations in vanadium spinels AV_2O_4 can be understood as a propagation of excitations to states with a given J_z through the crystal.

To proceed, we rewrite the Hamiltonian [Eq. (1)] as a sum of a single-ion Hamiltonian H_1 and the term which describes the interaction between two different ions H_2,

$$H = H_1 + H_2, \tag{9}$$

where

$$H_1 = H_{\mathrm{SO}} + H_a + \sum_i h_{zi} S_{zi},$$

$$H_2 = H_{\mathrm{SE}} - \sum_i h_{zi} S_{zi}. \tag{10}$$

The molecular field part of the exchange interaction acting on site i is given by $h_z=\Sigma_r Z_r J_r \langle S_z \rangle_r$. Z_r is the number of rth neighbors, J_r is the corresponding exchange constant, and $\langle S_z \rangle$ is the sublattice magnetization.

First, we diagonalize the single ion Hamiltonian H_1 in the molecular field approximation. It is convenient to express the eigenfunction $|J_z\rangle$ for the states splitted by the spin-orbit interaction as linear combinations of the unperturbed eigenfunctions of L'_z and S_z. Then, H_1 can be represented as a block 9×9 matrix in the subspace of $|L'_z, S_z\rangle$ as follows:

$$H_1(J_z = \pm 2) = c - \lambda \pm h_z, \tag{11}$$

$$H_1(J_z = \pm 1) = \begin{pmatrix} c & -\lambda \\ -\lambda & \pm h_z \end{pmatrix}, \tag{12}$$

$$H_1(J_z = 0) = \begin{pmatrix} c+\lambda-h_z & -\lambda & 0 \\ -\lambda & 0 & -\lambda \\ 0 & -\lambda & c+\lambda+h_z \end{pmatrix}, \tag{13}$$

where $J_z=2$, $J_z=-2$, $J_z=1$, $J_z=-1$, and $J_z=0$ are represented in the basis $|1,\ 1\rangle$, $|-1,-1\rangle$, $(|1,\ 0\rangle,\ |0,\ 1\rangle)$, $(|-1,0\rangle, |0,-1\rangle)$, and $(|1,-1\rangle,\ |0,\ 0\rangle,\ |-1,1\rangle)$, respectively. Diagonalizing these matrices, we obtain eigenvalues and eigenvectors of H_1 as functions of the molecular field h_z.

When the tetrahedra are flattened as observed in the experiments, i.e., when $c<0$, for any strength of the molecular field h_z, the ground state of H_1 has $J_z=\pm 2$ (the sign of J_z depends on the sign of h_z). For definiteness, we consider

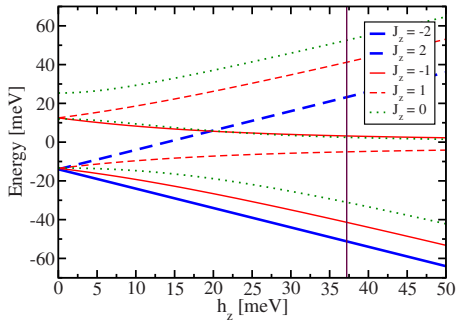

FIG. 4. (Color online) Energy levels of V^{3+} ions in AV_2O_4 as functions of molecular field h_z. $J_z=-2$ is a ground state for all values of h_z (solid blue bold line). The transitions are possible only to excited states with $J_z=-1$ (solid red thin lines).

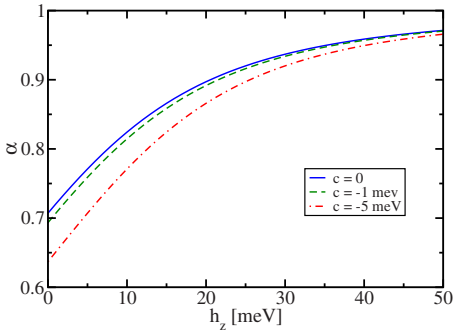

FIG. 5. (Color online) α as a function of molecular field h_z for different values of the tetragonal field c.

spin-down sublattice ($h_z>0$). The resulting energy levels are presented in Fig. 4. The magnetic excitations of the local Hamiltonian H_1 are transitions from the ground state to eight excited states of a single ion. These excitations can be described by boson operators $p_\nu^\dagger$—each pseudoboson describes the transition from the ground state $|0\rangle$ to the excited state $|\nu\rangle$. The single ion Hamiltonian H_1 is diagonal in terms of pseudoboson operators,

$$H_1 = \sum_i \sum_{\nu=1}^{8} \varepsilon_\nu p_{\nu i}^\dagger p_{\nu i}, \tag{14}$$

where ε_ν is the energy difference between the excited state $|\nu\rangle$ and the ground state of H_1,

$$\varepsilon_\nu = E_\nu - E_0. \tag{15}$$

We next introduce the representation for spin operators in terms of pseudobosons $p_\nu^\dagger$. The representation for spin $\mathbf{S}_p$ on the sublattice p can be written as

$$S_p^z = \langle 0|S_z|0\rangle + \sum_{\nu=1}^{8} \langle \nu|S_z|0\rangle (p_\nu^\dagger + p_\nu) + \sum_{\nu=1}^{8} (\langle \nu|S_z|\nu\rangle - \langle 0|S_z|0\rangle) p_\nu^\dagger p_\nu, \tag{16}$$

$$S_p^\pm = \sum_{\nu=1}^{8} (\langle \nu|S^\pm|0\rangle p_\nu^\dagger + \langle 0|S^\pm|\nu\rangle p_\nu). \tag{17}$$

If the ground state of H_1 corresponds to $J_z=-2$, it follows from Eq. (17) that only states with $J_z=-1$ contribute to $S_p^\pm$. There are two such states, $|1\rangle$ and $|2\rangle$. In the basis of $|L_z', S_z\rangle$, they have the following structure:

$$|1\rangle = \sqrt{1-\alpha^2}|-1,0\rangle + \alpha|0,-1\rangle,$$

$$|2\rangle = \alpha|-1,0\rangle - \sqrt{1-\alpha^2}|0,-1\rangle, \tag{18}$$

where we denote α as the weight of the state with $L_z'=0$, and $S_z=-1$ in the $|1\rangle$ state. The partial weight of orbital and spin contributions is determined by the competition between the spin-orbit coupling, the anisotropy energy, and the molecular exchange field. In Fig. 5, we present a dependence of α on the molecular exchange field h_z at different values of the tetragonal field c, keeping the SO coupling constant λ fixed. For all values of tetragonal field parameter, α shows similar field dependence: it increases with the increase of h_z. This happens because the molecular field h_z, acting on the spin S_i, is effectively created only by the nearest neighbors on the xy chain, which are antiferromagnetically aligned to S_i. Therefore, when h_z increases, the flipping of the spin costs more energy and the transitions with $\Delta S_z=1$ are suppressed. The low lying excitations become more of an orbital character, which can be seen in the increase of the weight of the transitions with $\Delta L_z'=1$.

As only two excited states of an ion are relevant to the spin-wave analysis, we consider the local excitations described by two pseudoboson operators $p_1^\dagger$ and $p_2^\dagger$, which take an ion from the ground state to states $|1\rangle$ and $|2\rangle$, respectively. The explicit form of extended Holstein-Primakoff transformation for spin $\mathbf{S}_p$ in terms p_1 and p_2 is given by

$$S_p^z = \langle 0|S_z|0\rangle + (\langle 1|S_z|1\rangle - \langle 0|S_z|0\rangle) p_1^\dagger p_1 + (\langle 2|S_z|2\rangle - \langle 0|S_z|0\rangle) p_2^\dagger p_2, \tag{19}$$

$$S_p^\pm = \langle 1|S^\pm|0\rangle p_1^\dagger + \langle 2|S^\pm|0\rangle p_2^\dagger + \langle 0|S^\pm|1\rangle p_1 + \langle 0|S^\pm|2\rangle p_2. \tag{20}$$

It is also useful to rewrite these expressions [Eqs. (19) and (20)] using the definition of α (for spin down),

$$S_p^z = -1 + (1-\alpha^2) p_1^\dagger p_1 + \alpha^2 p_2^\dagger p_2, \tag{21}$$

$$S_p^+ = \sqrt{(1-\alpha^2)2}\, p_1^\dagger + \alpha\sqrt{2} p_2^\dagger, \tag{22}$$

$$S_p^- = \sqrt{(1-\alpha^2)2}\, p_1 + \alpha\sqrt{2} p_2. \tag{23}$$

The interactions between localized excitations are described by H_2. The excitation spectrum is obtained in a similar way as in the spin wave analysis for the ROO state. After diagonalization, the total Hamiltonian $H=H_1+H_2$ can be written in the same form as Eq. (8); however, now the index n runs from 1 to 16 and the modes have complex spin-orbital character. The details of calculation are given in Appendix B.

The numerically calculated magnetic excitation spectrum for the COO state is presented in Fig. 6. For comparison, we

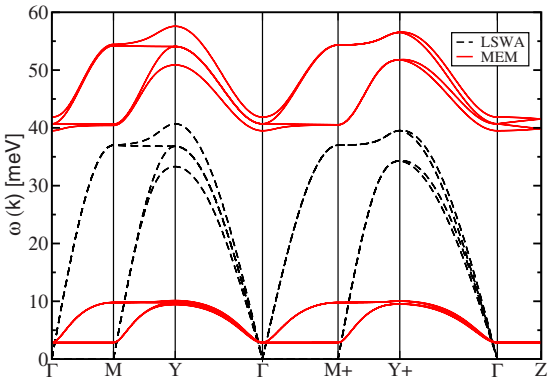

FIG. 6. (Color online) Magnetic excitation spectrum. Red solid lines correspond to magnetic excitations in the case of unquenched orbital angular momentum, $L \neq 0$, obtained in the framework of the magnetic exciton model. We use the following parameters: $J_{xy}=18.5$ meV, $J'=0.1J_{xy}$, $c=-1$ meV, and $\lambda=13$ meV. The black dashed lines correspond to pure spin waves, $L=0$, obtained in the linear spin wave approximation. The spectra are plotted along the same high-symmetry directions as in Fig. 2.

also plotted there the spin-wave dispersion for the ROO state. We used the following parameters: $J_{xy}=18.5$ meV, $J'=0.1J_{xy}$, $c=-1$ meV, and $\lambda=13$ meV (third neighbors interactions are not included here). As we see from Fig. 6, the excitation spectrum consists of eight different branches, each of them is doubly degenerate. The excitations may be divided into two groups: four low lying branches with rather small gap $\Delta_a \sim 3$ meV and four optical branches, with the gap $\Delta_o \sim 35$ meV. As $\Delta_a \ll \Delta_o$, the lying branches are quasiacoustic modes. As we see in Fig. 6, the lowest mode along the direction $\Gamma=(0,0,0) \rightarrow M=(\pi/4,\pi/4,0)$ is the dispersionless mode. This flat mode is a lifted "zero energy mode" of the ROO state. Here, the zero mode is lifted due to the combined effect of the anisotropy term and the SO coupling. The tetragonal distortion favors the nonzero value of the z component of orbital angular momentum, which, in turn, selects the local spin quantization axis in such a way that the z component of spin is nonzero. We found that the gap Δ_a is mainly determined by the anisotropy term and only weakly depends on the SO coupling (see Fig. 7).

However, we note once again, that, in principle, the lifting of zero energy mode can appear also in ROO state if single ion magnetic anisotropy is taken into account. We caution that the size of these two different anisotropy gaps can be of the same order, and therefore, it will be rather difficult to distinguish between them.

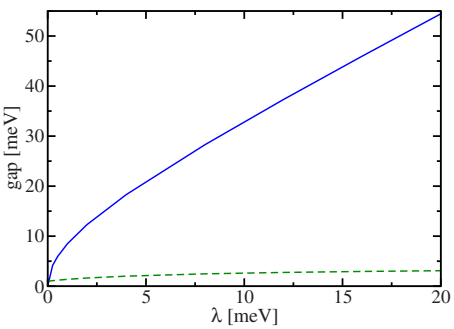

FIG. 7. (Color online) Anisotropy Δ_a (dashed line) and optical Δ_o (solid line) gaps as a function of spin-orbit coupling constant λ.

As a remark, we would like to mention that such lifted zero energy modes can be detected by an inelastic neutron scattering and have been indeed recently observed in the frustrated kagome lattice antiferromagnet $KFe_3(OH)_6(SO_4)_2$.[21]

There is another significant difference between the magnetic excitation spectrum for COO and ROO states: as one can see from Fig. 6, the bandwidth of quasiacoustic modes in the COO state is strongly reduced compared to the bandwidth of pure spin waves in the ROO state. This reduction is the effect of the mixing between orbital and pure spin excitations in the spectra of the COO state. Pure orbital excitations are nondispersive because they come from local interactions. The presence of the orbital component in the spin-wave spectrum then obviously leads to the reduction of the bandwidth.

We believe that this large reduction of the bandwidth can be seen experimentally in the neutron scattering measurements of the magnetic excitation spectrum. Such experimental results would discriminate between two types of orbital ordering, COO and ROO. Unfortunately, at present these experiments are difficult to perform because to measure the full spin-wave spectrum one needs single crystals, which are still not available as far as we know.

Let us now discuss the optical branches. These modes exist only in the COO state, and they arise from the hybridization between orbital angular momentum nondispersive levels and dispersive spin branches due to the spin-orbit coupling. In Fig. 5, we show how the optical gap Δ_o depends on the strength of the spin-orbit coupling. One can see that at $\lambda=0$, Δ_o is zero, but it rapidly increases with increasing λ.

To summarize, the magnetic excitation spectrum for the COO state has two separated branches: quasiacoustic modes and optical modes. Both manifolds are gapped, but the gaps Δ_a and Δ_o have different origins: Δ_a is set by the anisotropy term, while Δ_o is set by the spin-orbit coupling and is much larger.

These two gaps could be, in principle, determined by inelastic neutron or Raman scattering even in powder samples of ZnV_2O_4. They are also easily distinguishable from the well-known Haldane gap Δ_H, which is a characteristic feature of the antiferromagnetic $S=1$ chains. Δ_H, Δ_a, and Δ_o have different temperature dependence: the optical gap Δ_o does not depend on the temperature, as it is determined by the relativistic spin-orbit interaction; the anisotropy gap Δ_a is nonzero only below the temperature of the structural transition, $T<T_s$, and the Haldane gap should disappear below T_N, when a long range antiferromagnetic ordering emerges.

At all temperatures, the optical gap Δ_o is the largest, so we compare only the anisotropy and the Haldane gaps. At the lowest temperatures, $T<T_N$, the Haldane gap vanishes, and the lowest mode will have a gap equal to an anisotropy gap Δ_a. At intermediate temperatures, $T_N<T<T_S$, the spin excitations are also gapped. In this temperature range, the gap is the sum of the anisotropy gap Δ_a and the Haldane gap Δ_H. The magnitude of the well-developed Haldane gap is of the

order of $0.4J_{xy}$ and is compared to T_S; hence, it is very likely that the gap at $T_N < T < T_S$ will be larger than at low temperatures. This behavior is exotic and, as far as we know, has not been yet observed in $S=1$ spin-chain systems. At high temperatures, $T > T_S$, the sharp gap is washed out by thermal fluctuations, but the spectrum can still divided into acoustic and optical branches.

V. CONCLUSION

We presented in this paper a detail analysis of the magnetic excitations of vanadium spinels, whose low-temperature tetragonal phase can be modeled to a high accuracy by one-dimensional spin chains with weak interchain interaction. The formation of antiferromagnetic spin chains on the highly frustrated pyrochlore lattice is by itself nontrivial phenomena. This can happen only because vanadium ions also possess an orbital degree of freedom, and the orbital modulation of the spin exchange partially lifts the geometrical degeneracy of the underlying lattice.

We considered two different ground states: (i) the one with the real orbital ordering, ROO, and (ii) the one with the complex orbital ordering, COO. We found that the excitation spectra in these two cases are qualitatively different. The spectrum for the COO state consists of low lying quasiacoustic modes with small anisotropy gap and optical branches with zone-center gap determined by the spin-orbit coupling. The spectrum for the ROO state has only quasiacoustic modes. Within the superexchange model considered in the present study, the spectrum is gapless; however, in reality, we expect an anisotropy gap also for this state.

The bandwidth of the quasiacoustic modes in the COO state is strongly reduced compared to the ones for the ROO state, due to the contributions from orbital L modes. Because the spectra are so different, we argue that an effective way to determine experimentally the symmetry of orbital ordering in vanadium spinels is to measure their magnetic excitation spectrum.

ACKNOWLEDGMENTS

We gratefully acknowledge discussions with P. Fulde, A. Chubukov, S. Di Matteo, A. Loidl, H. Takagi, R. Valenti, and A. Yaresko.

APPENDIX A

In this appendix, we present the expressions for the matrices $\mathbf{A}(\mathbf{k})$ and $\mathbf{B}(\mathbf{k})$ in the Hamiltonian [Eq. (7)].

The diagonal elements of the matrix $\mathbf{A}(\mathbf{k})$ are given by

$$\mathbf{A}_{pp}(\mathbf{k}) = 2J_{xy} + 2J_3 \cos 2(k_x - k_y), \quad p = 1,3,5,7,$$

$$\mathbf{A}_{pp}(\mathbf{k}) = 2J_{xy} + 2J_3 \cos 2(k_x + k_y), \quad p = 2,4,6,8.$$

Nonzero matrix elements of $\mathbf{A}(\mathbf{k})$ are given by

$$\mathbf{A}_{14}(\mathbf{k}) = J' e^{-i(k_x - k_z)},$$

$$\mathbf{A}_{16}(\mathbf{k}) = J' e^{-i(k_y + k_z)},$$

$$\mathbf{A}_{23}(\mathbf{k}) = J' e^{-i(k_x + k_z)},$$

$$\mathbf{A}_{25}(\mathbf{k}) = J' e^{i(k_y + k_z)},$$

$$\mathbf{A}_{38}(\mathbf{k}) = J' e^{i(k_y - k_z)},$$

$$\mathbf{A}_{47}(\mathbf{k}) = J' e^{-i(k_y - k_z)},$$

$$\mathbf{A}_{58}(\mathbf{k}) = J' e^{-i(k_x - k_z)},$$

$$\mathbf{A}_{67}(\mathbf{k}) = J' e^{-i(k_x + k_z)},$$

$$\mathbf{A}_{pq}(\mathbf{k}) = \widetilde{\mathbf{A}}_{qp}(\mathbf{k}).$$

Nonzero matrix elements of $\mathbf{B}(\mathbf{k})$ are given by

$$\mathbf{B}_{13}(\mathbf{k}) = 2J_{xy} \cos(k_x - k_y),$$

$$\mathbf{B}_{24}(\mathbf{k}) = 2J_{xy} \cos(k_x + k_y),$$

$$\mathbf{B}_{57}(\mathbf{k}) = 2J_{xy} \cos(k_x - k_y),$$

$$\mathbf{B}_{68}(\mathbf{k}) = 2J_{xy} \cos(k_x + k_y),$$

$$\mathbf{B}_{12}(\mathbf{k}) = J' e^{i(k_y + k_z)},$$

$$\mathbf{B}_{18}(\mathbf{k}) = J' e^{i(k_x - k_z)},$$

$$\mathbf{B}_{27}(\mathbf{k}) = J' e^{i(k_x + k_z)},$$

$$\mathbf{B}_{34}(\mathbf{k}) = J' e^{-i(k_y - k_z)},$$

$$\mathbf{B}_{36}(\mathbf{k}) = J' e^{-i(k_x + k_z)},$$

$$\mathbf{B}_{45}(\mathbf{k}) = J' e^{-i(k_x - k_z)},$$

$$\mathbf{B}_{56}(\mathbf{k}) = J' e^{i(k_y + k_z)},$$

$$\mathbf{B}_{78}(\mathbf{k}) = J' e^{-i(k_y - k_z)},$$

$$\mathbf{B}_{15}(\mathbf{k}) = 2J_3 \cos 2(k_x - k_z),$$

$$\mathbf{B}_{26}(\mathbf{k}) = 2J_3 \cos 2(k_y - k_z),$$

$$\mathbf{B}_{37}(\mathbf{k}) = 2J_3 \cos 2(k_x + k_z),$$

$$\mathbf{B}_{48}(\mathbf{k}) = 2J_3 \cos 2(k_y - k_z),$$

$$\mathbf{B}_{pq}(\mathbf{k}) = \widetilde{\mathbf{B}}_{qp}(\mathbf{k}).$$

APPENDIX B

We next consider the modifications of the matrices for the exciton model.

In the exciton model, the base object is an enlarged set of pseudoboson operators $\hat{\mathbf{a}}(\mathbf{k})=[\mathbf{a}_1(\mathbf{k}),\mathbf{a}_2(\mathbf{k})]$, whose components $\mathbf{a}_1(\mathbf{k})$ and $\mathbf{a}_2(\mathbf{k})$ describe transitions to first and second excited levels. These two vectors are analogous to $\mathbf{a}(\mathbf{k})$ for pure spin wave model. As a result, the matrix $\mathbf{A}(\mathbf{k})$ is enlarged and becomes a 16×16 matrix $\hat{\mathbf{A}}(\mathbf{k})$. Its components are given by

$$\hat{\mathbf{A}}(\mathbf{k})=\begin{pmatrix}(1-\alpha^2)\mathcal{A}(\mathbf{k})+\varepsilon_1 & \alpha\sqrt{1-\alpha^2}\mathcal{A}(\mathbf{k})\\ \alpha\sqrt{1-\alpha^2}\mathcal{A}(\mathbf{k}) & \alpha^2\mathcal{A}(\mathbf{k})+\varepsilon_2\end{pmatrix}, \quad \text{(B1)}$$

where

$$\mathcal{A}_{pq}(\mathbf{k})=\begin{cases}\mathbf{A}_{pq}(\mathbf{k}), & p\neq q\\ 0, & p=q.\end{cases} \quad \text{(B2)}$$

Here, p and q runs from 1 to 8. The diagonal matrix elements of $\mathcal{A}_{pq}(\mathbf{k})$ are zero (we consider only the case $J_3=0$) because the diagonal contribution is already included in ε_ν.

Similarly, we can obtain the expression for the matrix $\hat{\mathbf{B}}(\mathbf{k})$,

$$\begin{pmatrix}(1-\alpha^2)\mathbf{B}(\mathbf{k}) & \alpha\sqrt{1-\alpha^2}\mathbf{B}(\mathbf{k})\\ \alpha\sqrt{1-\alpha^2}\mathbf{B}(\mathbf{k}) & \alpha^2\mathbf{B}(\mathbf{k})\end{pmatrix}. \quad \text{(B3)}$$

[1] Y. Ueda, N. Fujiwara, and H. Yasuoka, J. Phys. Soc. Jpn. **66**, 778 (1997).
[2] S. Nizioł, Phys. Status Solidi A **18**, K11 (1973).
[3] M. Reehuis, A. Krimmel, N. Büttgen, A. Loidl, and A. Prokofiev, Eur. Phys. J. B **35**, 311 (2003).
[4] M. Muhtar, F. Takagi, K. Kawakami, and N. Tsuda, J. Phys. Soc. Jpn. **57**, 3119 (1988).
[5] S.-H. Lee *et al.*, Phys. Rev. Lett. **93**, 156407 (2004).
[6] Y. Yamashita and K. Ueda, Phys. Rev. Lett. **85**, 4960 (2000).
[7] H. Tsunetsugu and Y. Motome, Phys. Rev. B **68**, 060405(R) (2003); Y. Motome and H. Tsunetsugu, *ibid.* **70**, 184427 (2004).
[8] O. Tchernyshyov, Phys. Rev. Lett. **93**, 157206 (2004).
[9] T. Maitra and R. Valenti, Phys. Rev. Lett. **99**, 126401 (2007).
[10] S. Di Matteo, G. Jackeli, and N. B. Perkins, Phys. Rev. B **72**, 020408(R) (2005).
[11] In relation to previous works, the consideration in Ref. 7 corresponds to $L=0$, while the one in Refs. 8 and 10 corresponds to $L\neq 0$.
[12] C. J. Ballhausen, *Introduction to Ligand Field Theory* (McGraw-Hill, New York, 1962), p. 89.
[13] K. Takubo, J.-Y. Son, T. Mizokawa, H. Ueda, M. Isobe, Y. Matsushita, and Y. Ueda, Phys. Rev. B **74**, 155103 (2006).
[14] T. Mizokawa and A. Fujimori, Phys. Rev. B **54**, 5368 (1996).
[15] A. Abragam and B. Bleaney, *Introduction to Ligand Field Theory* (Clarendon, Oxford, 1970), pp. 377–378 and 426–429.
[16] L. R. Walker, in *Magnetism*, edited by G. T. Rado and H. H. Suhl (Academic, New York, 1963), Vol. 1, pp. 299–381.
[17] Y. Motome and H. Tsunetsugu, Prog. Theor. Phys. Suppl. **160**, 203 (2005).
[18] We would like to note that the coupling between third neighbors arises not only due to the direct exchange but also due to the various superexchange paths through oxygen ions. In some pyrochlore compounds, this contribution can be rather significant, however, here, for simplicity, we did not take this coupling into account.
[19] W. J. L. Buyers, T. M. Holden, E. C. Svensson, R. A. Cowley, and M. T. Hutchings, J. Phys. C **4**, 2139 (1971).
[20] K. Tomiyasu and S. Itoh, J. Phys. Soc. Jpn. **75**, 084708 (2006).
[21] K. Matan, D. Grohol, D. G. Nocera, T. Yildirim, A. B. Harris, S. H. Lee, S. E. Nagler, and Y. S. Lee, Phys. Rev. Lett. **96**, 247201 (2006).